



## Aberystwyth University

### *Controlling the growth of epitaxial graphene on metalized diamond (111) surface*

Cooil, Simon Phillip; Wells, J. W.; Hu, Di; Niu, Y. R.; Zakharov, A. A.; Bianchi, M.; Evans, D. A.

*Published in:*

Applied Physics Letters

*DOI:*

[10.1063/1.4935073](https://doi.org/10.1063/1.4935073)

*Publication date:*

2015

*Citation for published version (APA):*

Cooil, S. P., Wells, J. W., Hu, D., Niu, Y. R., Zakharov, A. A., Bianchi, M., & Evans, D. A. (2015). Controlling the growth of epitaxial graphene on metalized diamond (111) surface. *Applied Physics Letters*, 107(18), [181603]. <https://doi.org/10.1063/1.4935073>

#### Document License

CC BY-NC

#### General rights

Copyright and moral rights for the publications made accessible in the Aberystwyth Research Portal (the Institutional Repository) are retained by the authors and/or other copyright owners and it is a condition of accessing publications that users recognise and abide by the legal requirements associated with these rights.

- Users may download and print one copy of any publication from the Aberystwyth Research Portal for the purpose of private study or research.
- You may not further distribute the material or use it for any profit-making activity or commercial gain
- You may freely distribute the URL identifying the publication in the Aberystwyth Research Portal

#### Take down policy

If you believe that this document breaches copyright please contact us providing details, and we will remove access to the work immediately and investigate your claim.

tel: +44 1970 62 2400

email: [is@aber.ac.uk](mailto:is@aber.ac.uk)

## Controlling the growth of epitaxial graphene on metalized diamond (111) surface

S. P. Cooil, J. W. Wells, D. Hu, Y. R. Niu, A. A. Zakharov, M. Bianchi, and D. A. Evans

Citation: [Applied Physics Letters](#) **107**, 181603 (2015); doi: 10.1063/1.4935073

View online: <http://dx.doi.org/10.1063/1.4935073>

View Table of Contents: <http://scitation.aip.org/content/aip/journal/apl/107/18?ver=pdfcov>

Published by the [AIP Publishing](#)

---

### Articles you may be interested in

[Structural and electronic properties of multilayer graphene on monolayer hexagonal boron nitride/nickel \(111\) interface system: A van der Waals density functional study](#)

[J. Appl. Phys.](#) **119**, 065307 (2016); 10.1063/1.4941552

[Step edge influence on barrier height and contact area in vertical heterojunctions between epitaxial graphene and n-type 4H-SiC](#)

[Appl. Phys. Lett.](#) **104**, 073508 (2014); 10.1063/1.4866024

[A route to strong p-doping of epitaxial graphene on SiC](#)

[Appl. Phys. Lett.](#) **97**, 193304 (2010); 10.1063/1.3515848

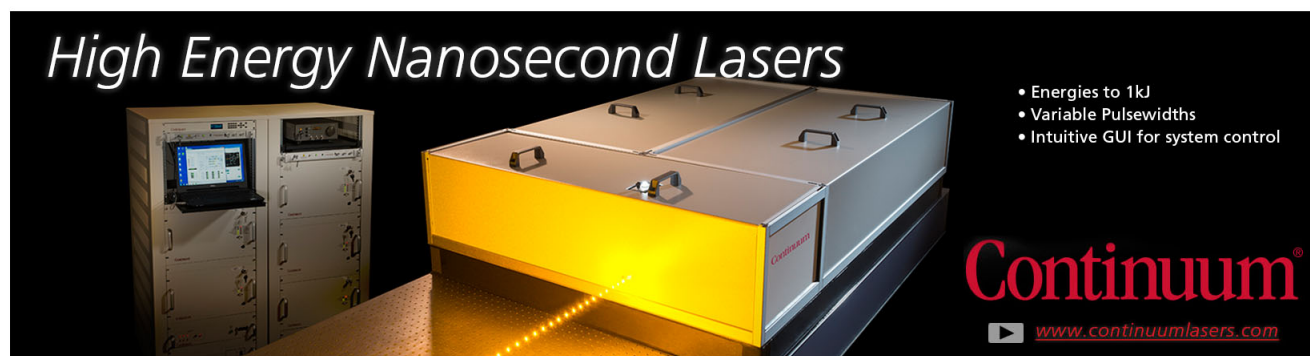
[Growth kinetics, structure, and morphology of para-quaterphenyl thin films on gold\(111\)](#)

[J. Chem. Phys.](#) **121**, 2272 (2004); 10.1063/1.1767154

[Epitaxial growth of pentacene films on Cu\(110\)](#)

[J. Chem. Phys.](#) **121**, 525 (2004); 10.1063/1.1760076

---

An advertisement for Continuum High Energy Nanosecond Lasers. The image shows a rack of laser control units on the left and a large, rectangular laser unit on the right that is emitting a bright yellow laser beam. The text 'High Energy Nanosecond Lasers' is written in a white, italicized font at the top left. On the right side, there is a list of features: 'Energies to 1kJ', 'Variable Pulsewidths', and 'Intuitive GUI for system control'. The Continuum logo is in red at the bottom right, with the website 'www.continuumlasers.com' below it.

*High Energy Nanosecond Lasers*

- Energies to 1kJ
- Variable Pulsewidths
- Intuitive GUI for system control

**Continuum**<sup>®</sup>

[www.continuumlasers.com](http://www.continuumlasers.com)

## Controlling the growth of epitaxial graphene on metalized diamond (111) surface

S. P. Cooil,<sup>1,2,a)</sup> J. W. Wells,<sup>2</sup> D. Hu,<sup>1</sup> Y. R. Niu,<sup>3</sup> A. A. Zakharov,<sup>3</sup> M. Bianchi,<sup>4</sup> and D. A. Evans<sup>1</sup>

<sup>1</sup>*Department of Physics, Aberystwyth University, Aberystwyth SY23 3BZ, United Kingdom*

<sup>2</sup>*Department of Physics, Norwegian University of Science and Technology (NTNU), Høgskoleringen 5, 7491 Trondheim, Norway*

<sup>3</sup>*MAX IV Laboratory, Lund University, 221 00 Lund, Sweden*

<sup>4</sup>*Department of Physics and Astronomy and Interdisciplinary Nanoscience Center, Aarhus University, Aarhus DK-8000, Denmark*

(Received 8 May 2015; accepted 29 September 2015; published online 3 November 2015)

The 2-dimensional transformation of the diamond (111) surface to graphene has been demonstrated using ultrathin Fe films that catalytically reduce the reaction temperature needed for the conversion of sp<sup>3</sup> to sp<sup>2</sup> carbon. An epitaxial system is formed, which involves the re-crystallization of carbon at the Fe/vacuum interface and that enables the controlled growth of monolayer and multilayer graphene films. In order to study the initial stages of single and multilayer graphene growth, real time monitoring of the system was performed within a photoemission and low energy electron microscope. It was found that the initial graphene growth occurred at temperatures as low as 500 °C, whilst increasing the temperature to 560 °C was required to produce multi-layer graphene of high structural quality. Angle resolved photoelectron spectroscopy was used to study the electronic properties of the grown material, where a graphene-like energy momentum dispersion was observed. The Dirac point for the first layer is located at 2.5 eV below the Fermi level, indicating an n-type doping of the graphene due to substrate interactions, while that of the second graphene layer lies close to the Fermi level. © 2015 AIP Publishing LLC.

[<http://dx.doi.org/10.1063/1.4935073>]

Since its discovery,<sup>1,2</sup> graphene's electronic properties have been applied in areas such as photovoltaic devices,<sup>3</sup> quantum-electronics,<sup>4</sup> and gas sensing.<sup>5</sup> The material quality required for these applications defines the fabrication method and these include exfoliation, reduction of graphene oxide,<sup>6</sup> chemical vapour deposition (CVD),<sup>7</sup> sublimation of Si from SiC substrates,<sup>8</sup> and solid-state transformation of amorphous carbon through catalytically active metals.<sup>9,10</sup> Where single crystal material is required, for example, to minimise grain boundaries,<sup>11</sup> the fabrication methods often require many substrate processing steps<sup>12</sup> or high temperatures.<sup>13</sup> Here, we demonstrate that we are able to process monolayer graphene (MLG) and few layer graphene (FLG) films in the solid state directly onto substrates that have already shown potential for spin-based electronics. For example, graphene demonstrates very long spin-coherence lengths,<sup>14,15</sup> which when coupled to the long spin storage times available in diamond nitrogen-vacancy (NV) centers,<sup>16</sup> could lead to a potentially interesting platform for future applications such as quantum computing.

The process involves the catalytic detachment of carbon from a diamond (111) surface in the presence of a thin Fe film, without which temperatures in excess of 1000 °C would be required.<sup>17</sup> The process differs, for example, from methods of metal-catalysed graphene growth from amorphous carbon on SiO<sub>2</sub> substrates,<sup>9,10</sup> in that the carbon here is in the form of a highly crystalline hexagonal diamond (111) surface, which provides the source of carbon and a structural

template that is closely matched to the lattice of both the metal and the graphene. The catalytic effect of Fe in carbon chemistry has been widely studied in the production of carbon nanotubes. Conversely Ni and Co<sup>18–20</sup> have received more attention than Fe as substrates for graphene growth, largely due to the formation of undesirable iron carbide phases. However, in a study of the low temperature CVD growth of graphene on Fe(110) substrates, Vinogradov *et al.*<sup>21</sup> used a reduced temperature to inhibit carbide formation whilst still providing sufficient thermal energy to promote the catalytic action of the Fe layer. We have previously shown that interfacial carbide formation does not prevent the formation of graphene on the metalized surface of diamond and SiC,<sup>20</sup> and we now confirm the high structural and electronic quality of the single and bilayer films using synchrotron-based photoelectron methods.

The chemical composition and morphology of the surface was investigated at MAXLab<sup>22</sup> using X-ray photoemission electron microscopy (XPEEM) and low energy electron microscopy (LEEM). Selective area low energy electron diffraction ( $\mu$ LEED) was used to investigate the localised crystalline quality along with selective area core-level X-ray photoelectron spectroscopy ( $\mu$ XPS) to probe the local chemical state. Additional low energy electron reflectivity (LEER) spectra provided an accurate method to detect the number of graphene layers grown. Using the optimised growth parameters determined from these methods, the electronic band structure of MLG and FLG films was determined by angle resolved photoelectron spectroscopy (ARPES) at the centre for storage ring facilities, Aarhus.<sup>23</sup>

<sup>a)</sup>Electronic mail: simon.cooil@ntnu.no

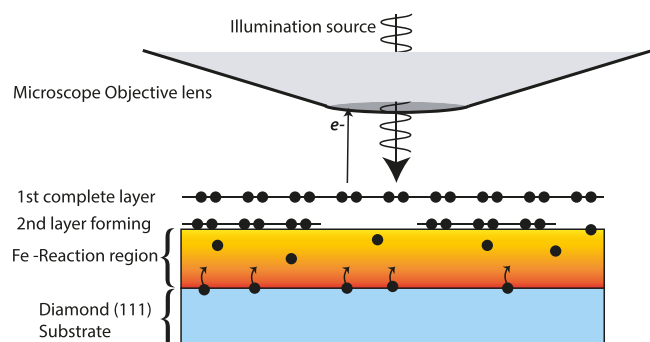


FIG. 1. A schematic representation of the system under investigation. Carbon atoms are catalytically detached from the diamond surface and transported through the Fe film to the Fe-vacuum interface where they recrystallize to form graphene. Following the completion of the first graphene layer, subsequent growth occurs from underneath. In this particular microscope, the illumination electrons and X-rays both impinge on the surface at normal incidence.

The substrate used in all studies was a natural type-IIb single crystal diamond with a low miscut angle to the (111) plane. In order to prepare a surface free of contamination and to remove Fe between investigations, a sulphuric acid and potassium nitrate etch was performed, leaving the surface oxygen terminated as a result. The chemical composition was confirmed by XPS and the root-mean squared surface roughness was found to be  $<1$  nm across the diamond surface by non-contact mode atomic force microscopy (AFM) (see the supplementary material).<sup>24</sup> A clean, oxygen-free surface was required before Fe deposition; therefore, the sample was annealed in the ultrahigh vacuum environment at  $1000^\circ\text{C}$ . XPS measurements confirmed the lack of oxygen, and a  $2 \times 1$  surface reconstruction was observed in LEED. For Fe growth, a  $1 \times 1$  surface is desired; therefore, the sample was exposed to an atomic hydrogen environment (plasma or hot filament cracking) at  $\sim 400^\circ\text{C}$  until the  $1 \times 1$  LEED pattern was recovered. The diamond surface prepared in this way provides the substrate for all further graphene growth studies.

A schematic representation of the system under investigation is shown in Figure 1. Thin and homogenous Fe films

were grown at room temperature at vacuum pressures  $<1 \times 10^{-9}$  mbar using an e-beam evaporator (Omicron EFM 3). Calibrated growth rates of  $0.02$ – $0.1$  nm  $\text{min}^{-1}$  were typically used. A 2 nm Fe film was found to completely suppress the C1s core level emission signal from the diamond when irradiated by synchrotron radiation of energy 330 eV, indicating a uniform 2-d layer was formed.<sup>24</sup>

Carbon emerging at the Fe-vacuum interface was initially detected by XPS at a temperature of  $490^\circ\text{C}$  as shown in Figure 2(d). This promotion of carbon to the metal surface was accompanied by an increased surface roughening as shown by LEEM image in Figure 2(a). Further annealing of this sample at  $500^\circ\text{C}$  resulted in the smoothing of the surface as shown in the sequence of LEEM images presented in Figures 2(a)–2(c). The homogeneous image of Figure 2(c) suggests that a complete layer of graphene was formed after a 90 min anneal at this temperature. This layer extended across the entire measurable crystal surface and had few small defects ( $<1 \mu\text{m}$ ). The resultant LEED pattern of this surface (Figure 2(e)) is the bright hexagonal  $1 \times 1$  LEED pattern of single-domain, epitaxial graphene. There is a weak Moiré pattern around the diffraction spots, which extends along the  $[1\bar{1}0]$  direction, indicating some long-range order between the graphene and the underlying Fe-film. The LEER spectrum of the surface (Figure 2(f)) shows a strong energy dependence with a minimum at  $\sim 0.5$  eV. LEER simulations of graphene on copper<sup>25</sup> suggest that the energy position of this minimum depends on the substrate-graphene separation with values of  $<1$  eV corresponding to  $>4.5 \text{ \AA}$ .

At temperatures above  $500^\circ\text{C}$ , small FLG islands were found to grow on the first graphene layer. The occurrence of these FLG islands appears to be correlated with defects in the first complete graphene layer. Increasing the substrate temperature to  $540^\circ\text{C}$  in  $20^\circ\text{C}$  steps with measurements performed at room temperature following each step, resulted in the growth of the FLG islands ( $\sim 10 \mu\text{m}$ ), as illustrated by the regions of different contrast in the LEEM image of Figure

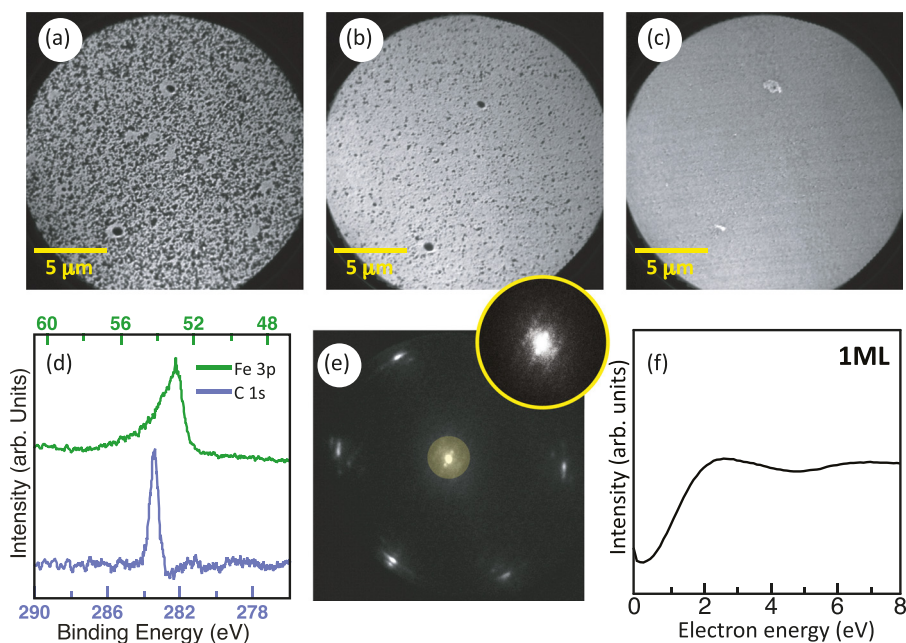


FIG. 2. LEEM images (a)–(c) were recorded during a 90 min anneal of a metalized diamond (111) surface at  $500^\circ\text{C}$  for 1, 15, and 90 min, respectively, following prior annealing to  $490^\circ\text{C}$ . The microscope field of view was  $20 \mu\text{m}$  with electron energy of  $10.3$ – $11.2$  eV. The  $\mu\text{XPS}$  spectra shown in (d) are C 1s and Fe 3p photoelectron peaks recorded at the onset of graphene formation. The LEED pattern (e) for an incident electron energy,  $E_{\text{kin}} = 50$  eV, was typical for the entire surface. LEER spectrum (f) of the final surface suggests a single layer of graphene.

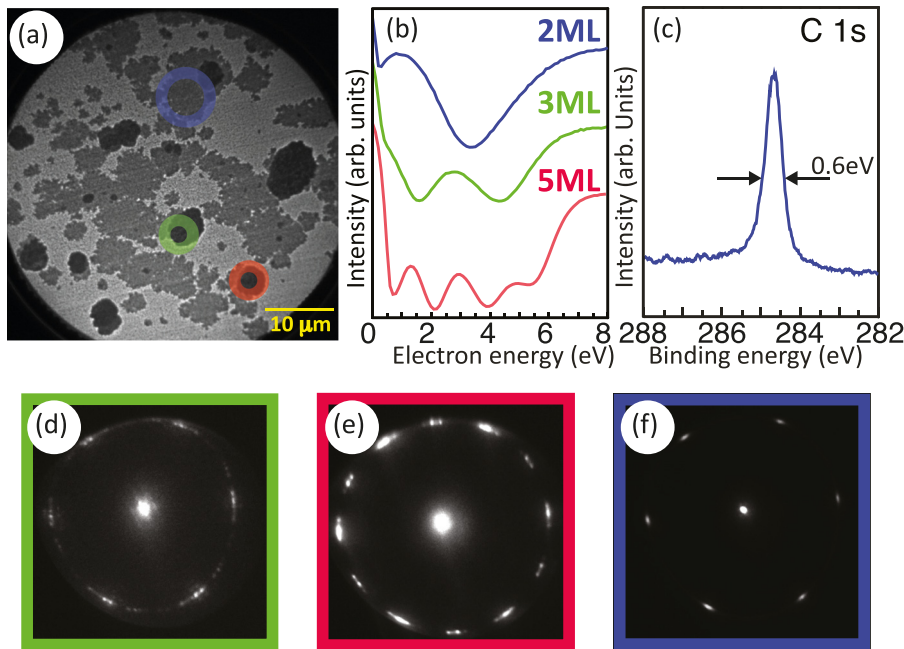


FIG. 3. LEEM study of the surface following further annealing steps: (a) LEEM image ( $E_{kin}=4.7$  eV) for a metalized diamond (111) surface following numerous anneal cycles at temperatures up to 560 °C. (b) LEER reflectivity spectra for selected areas of the annealed surface with different graphene layers. (c) C 1s core level photoelectron spectrum for the 2 ML region. (d)–(f) show LEED patterns for selected graphene islands of 3 ML (green), 5 ML (red), and 2 ML (blue), respectively. Colours throughout the figure correspond to the coloured circles in panel (a).

3(a). The number of minima in the LEER spectra for selected areas of different LEEM contrast corresponds to the number of graphene layers in these FLG islands<sup>25,26</sup> (Figure 3(b)). The smaller, darker regions (green and red circles) in Figure 3(a) therefore corresponds to 3 and 5 graphene layers, respectively in this example, although islands of a range of thicknesses were observed across the sample surface.

The characteristic asymmetric C 1s core level line-shape for  $sp^2$ -bonded carbon (Figure 3(c)) was measured at all points on the surface with the narrow FWHM indicating a well-ordered crystal.<sup>27</sup>

The  $\mu$ LEED patterns of the 3 and 5 layer regions that formed during the annealing steps to 540 °C (Figures 3(d) and 3(e)) show rotational domain variations within the layers. However, the large regions of 2 ML graphene (blue circle) that were formed following a further anneal step to 560 °C grew in a single-domain structure as shown in the  $\mu$ LEED pattern of Figure 3(f). This 2-D layer originated from a large number of small (<100 nm) areas that merged laterally to form a second epitaxial graphene layer above the first graphene layer, as described in Figure 2. This is interpreted to be the result of a new graphene layer forming at the Fe/Graphene interface, promoting regions of the first complete layer to the surface. The lightest regions in Figure 3(a) correspond to the graphene identical to that shown in Figure 2(c).

Having confirmed the structural and compositional quality of the graphene films and defining the parameters for 2-d growth, this method was used to prepare high quality graphene layers for further study of the electronic band structure. A 2 ML graphene film grown by the prolonged annealing of a Fe–diamond(111) interface at 500 °C, followed by a rapid increase to 560 °C, was prepared for ARPES measurements.

The ARPES measurement in Figure 4(a) shows the measured photoelectron intensity in the graphene  $\pi$ -bands nearest to the Fermi level ( $E_F$ ) along the  $\bar{K} - \bar{M} - \bar{K}'$  direction of the Brillouin zone. The binding energies of the

$\pi$ -band at the  $\bar{K}$  and  $\bar{M}$  points are found by taking energy dependent curves (EDCs) at these two points (0.8 and 0  $\text{\AA}^{-1}$ , respectively). The EDCs are shown adjacent to the schematic of Figure 4(b). Two clear graphene-like  $\pi$ -bands can be seen, illustrated schematically (red and blue curves), along with two Fe 3d bands (orange) in Figure 4(b).

The higher binding energy band in Figure 4(a) is related to the first graphene layer.<sup>24</sup> The Dirac-point and the saddle point of the  $\pi$ -band lie at 2.5 eV and 4.7 eV below the  $E_F$ , respectively. This band belongs to the graphene located at the Fe/Graphene interface and suggests a very strong n-type doping of the graphene due to interaction with the Fe film. The  $\pi^*$ -bands of this monolayer are seen to intersect with the Fe 3d states at around 1.5 eV and are not observed at lower binding energies. Hybridisation of the metal 3d-states and the  $\pi^*$ -states of graphene has been reported to induce a band-gap opening in the conduction band in ARPES studies of graphene on other transition metals such as Ni, Co,<sup>28</sup> and other Fe-graphene systems.<sup>19</sup> This points to a possible reason as to why the  $\pi^*$ -states of the first graphene layer are not observed following their intersection with the metal 3d-states.

The  $\pi$ -band of the graphene that has been promoted to the surface intersects with  $E_F$  near the Dirac point, characteristic of the electron dispersion of pristine graphene.<sup>29</sup> Interactions between graphene layers in FLG films have been shown to result in a change in the electronic dispersion of the  $\pi$ -band close to the Dirac point,<sup>30,31</sup> resulting in a non-linearity. In our measurements, the electronic dispersion of the  $\pi$ -band near the Dirac point of each graphene layer still exhibits a linear relation, indicating that the interaction between the two layers is weak.

In summary, a controllable method for the epitaxial growth of large area monolayer and bilayer graphene, using catalytic thermal decomposition of a diamond-Fe interface has been demonstrated. Graphene growth was found to initiate at temperatures as low as 500 °C, although it was self-limiting at one monolayer at this temperature. As with most methods of graphene fabrication, the electronic structure of the

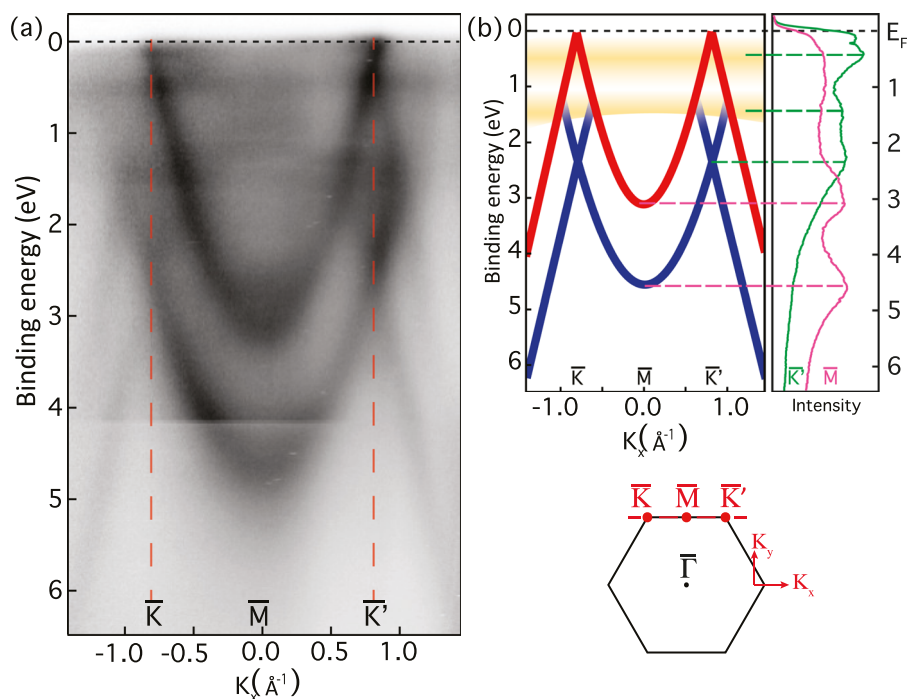


FIG. 4. (a) Measured photoelectron intensity along the  $\bar{K} - \bar{M} - \bar{K}'$  direction of the Brillouin zone of a 2 ML graphene film grown on a metalized diamond(111) surface. (b) Schematic representation of the data shown in (a) with the binding energies of the high symmetry points referenced to the peak positions of the EDCs extracted at  $\bar{K}'$  (green) and  $\bar{M}$  (pink) in the adjacent panel.  $h\nu = 45$  eV, 0 eV is referenced to the Fermi-level of a clean Au crystal.

graphene layer in closest proximity to the substrate is influenced by substrate interactions,<sup>32,33</sup> which is indeed the case here.

Rapidly increasing the temperature from 500 °C to 560 °C promotes the 2-D growth of a second epitaxial graphene layer forming below the first, promoting the first complete layer to the surface. The electron dispersion of this layer now shows the characteristic band structure of quasi-freestanding graphene, indicating only small or negligible interaction with the newly formed layer at the graphene/Fe interface.

Commercially produced diamond of extremely high quality is now manufactured routinely. Control over the number of NV defects is also attainable<sup>34</sup> and is the key reason behind diamond's quick emergence as an exciting spintronic material. When coupled to other already distinguished spin transport and injection materials, such as graphene and ferromagnetic Fe, the possibility for further fundamental investigation and potential applications is apparent.

The authors would like to acknowledge the financial support from the EPSRC (EP/G068216/1) and the HEFCW-funded Centre for Advanced Functional Materials and Devices. The authors would also like to thank Stephen Evans, Zhongfu Zhou, Philip Hofmann, and Alexei Preobrajenski for many fruitful discussions and practical advice.

<sup>1</sup>A. K. Geim and K. S. Novoselov, *Nat. Mater.* **6**(3), 183–191 (2007).

<sup>2</sup>K. S. Novoselov, A. K. Geim, S. V. Morozov, D. Jiang, Y. Zhang, S. V. Dubonos, I. V. Grigorieva, and A. A. Firsov, *Science* **306**(5696), 666–669 (2004).

<sup>3</sup>H. Park, J. A. Rowehl, K. K. Kim, V. Bulovic, and J. Kong, *Nanotechnology* **21**(50), 505204 (2010).

<sup>4</sup>M. Dragoman and D. Dragoman, *Prog. Quantum Electron.* **33**(6), 165–214 (2009).

<sup>5</sup>S. Ruyantsev, G. Liu, M. S. Shur, R. A. Potyrailo, and A. A. Balandin, *Nano Lett.* **12**(5), 2294–2298 (2012).

<sup>6</sup>H. A. Becerril, J. Mao, Z. Liu, R. M. Stoltenberg, Z. Bao, and Y. Chen, *ACS Nano* **2**(3), 463–470 (2008).

<sup>7</sup>J. Winterlin and M. L. Bocquet, *Surf. Sci.* **603**(10–12), 1841–1852 (2009).

<sup>8</sup>S. Forti, K. V. Emtsev, C. Coletti, A. A. Zakharov, C. Riedl, and U. Starke, *Phys. Rev. B* **84**(12), 125449 (2011).

<sup>9</sup>J. A. Rodríguez-Manzo, C. Pham-Huu, and F. Banhart, *ACS Nano* **5**(2), 1529–1534 (2011).

<sup>10</sup>M. Zheng, K. Takei, B. Hsia, H. Fang, X. Zhang, N. Ferralis, H. Ko, Y.-L. Chueh, Y. Zhang, R. Maboudian, and A. Javey, *Appl. Phys. Lett.* **96**(6), 063110 (2010).

<sup>11</sup>H. Zhang, G. Lee, C. Gong, L. Colombo, and K. Cho, *J. Phys. Chem. C* **118**(5), 2338–2343 (2014).

<sup>12</sup>H. Zhou, W. J. Yu, L. Liu, R. Cheng, Y. Chen, X. Huang, Y. Liu, Y. Wang, Y. Huang, and X. Duan, *Nat. Commun.* **4**, 2096 (2013).

<sup>13</sup>L. Gao, J. R. Guest, and N. P. Guisinger, *Nano Lett.* **10**(9), 3512–3516 (2010).

<sup>14</sup>T. Y. Yang, J. Balakrishnan, F. Volmer, A. Avsar, M. Jaiswal, J. Samm, S. R. Ali, A. Pachoud, M. Zeng, M. Popinciuc, G. Güntherodt, B. Beschoten, and B. Özyilmaz, *Phys. Rev. Lett.* **107**(4), 047206 (2011).

<sup>15</sup>W. Han and R. K. Kawakami, *Phys. Rev. Lett.* **107**(4), 047207 (2011).

<sup>16</sup>L. Childress, M. V. Gurudev Dutt, J. M. Taylor, A. S. Zibrov, F. Jelezko, J. Wrachtrup, P. R. Hemmer, and M. D. Lukin, *Science* **314**(5797), 281–285 (2006).

<sup>17</sup>T. Norio, F. Makoto, M. Toshiharu, T. Daisuke, Y. Satoshi, and I. Takao, *Jpn. J. Appl. Phys., Part 1* **52**(11R), 110121 (2013).

<sup>18</sup>Y. Xue, B. Wu, Y. Guo, L. Huang, L. Jiang, J. Chen, D. Geng, Y. Liu, W. Hu, and G. Yu, *Nano Res.* **4**(12), 1208–1214 (2011).

<sup>19</sup>A. Varykhalov, J. Sanchez-Barriga, P. Hlawenka, and O. Rader, e-print [arXiv:1212.6866](https://arxiv.org/abs/1212.6866).

<sup>20</sup>S. P. Cooil, F. Song, G. T. Williams, O. R. Roberts, D. P. Langstaff, B. Jørgensen, K. Høydaalsvik, D. W. Breiby, E. Wahlström, D. A. Evans, and J. W. Wells, *Carbon* **50**(14), 5099–5105 (2012).

<sup>21</sup>N. A. Vinogradov, A. A. Zakharov, V. Kocovski, J. Ruzs, K. A. Simonov, O. Eriksson, A. Mikkelsen, E. Lundgren, A. S. Vinogradov, N. Mårtensson, and A. B. Preobrajenski, *Phys. Rev. Lett.* **109**(2), 026101 (2012).

<sup>22</sup>A. A. Zakharov, A. Mikkelsen, and J. N. Andersen, *J. Electron Spectrosc. Relat. Phenom.* **185**(10), 417–428 (2012).

<sup>23</sup>S. V. Hoffmann, C. Søndergaard, C. Schultz, Z. Li, and P. Hofmann, *Nucl. Instrum. Methods Phys. Res., Sect. A* **523**(3), 441–453 (2004).

<sup>24</sup>See supplementary material at <http://dx.doi.org/10.1063/1.4935073> for further details of the sample preparation, first layer graphene growth, and AFM characterization.

<sup>25</sup>N. Srivastava, Q. Gao, M. Widom, R. M. Feenstra, S. Nie, K. F. McCarty, and I. V. Vlasiouk, *Phys. Rev. B* **87**(24), 245414 (2013).

<sup>26</sup>H. Hibino, H. Kageshima, F. Maeda, M. Nagase, Y. Kobayashi, and H. Yamaguchi, *Phys. Rev. B* **77**(7), 075413 (2008).

<sup>27</sup>S. Evans and J. M. Thomas, *Proc. R. Soc. London, Ser. A* **353**(1672), 103–120 (1977).

- <sup>28</sup>A. Varykhalov, D. Marchenko, J. Sánchez-Barriga, M. R. Scholz, B. Verberck, B. Trauzettel, T. O. Wehling, C. Carbone, and O. Rader, *Phys. Rev. X* **2**(4), 041017 (2012).
- <sup>29</sup>N. A. Vinogradov, K. A. Simonov, A. A. Zakharov, J. W. Wells, A. V. Generalov, A. S. Vinogradov, N. Martensson, and A. B. Preobrajenski, *Appl. Phys. Lett.* **102**(6), 061601–061605 (2013).
- <sup>30</sup>A. H. Castro Neto, F. Guinea, N. M. R. Peres, K. S. Novoselov, and A. K. Geim, *Rev. Mod. Phys.* **81**(1), 109–162 (2009).
- <sup>31</sup>K. F. Mak, J. Shan, and T. F. Heinz, *Phys. Rev. Lett.* **104**(17), 176404 (2010).
- <sup>32</sup>G. Giovannetti, P. A. Khomyakov, G. Brocks, V. M. Karpan, J. van den Brink, and P. J. Kelly, *Phys. Rev. Lett.* **101**(2), 026803 (2008).
- <sup>33</sup>A. Grüneis and D. V. Vyalikh, *Phys. Rev. B* **77**(19), 193401 (2008).
- <sup>34</sup>M. L. Markham, J. M. Dodson, G. A. Scarsbrook, D. J. Twitchen, G. Balasubramanian, F. Jelezko, and J. Wrachtrup, *Diamond Relat. Mater.* **20**(2), 134–139 (2011).